Structure ordering and glass transition in size-asymmetric ternary mixtures of hard spheres: Variation from fragile to strong glasses

Ankit Singh ⬤ and Yashwant Singh ⬤

Department of Physics, Banaras Hindu University, Varanasi 221 005, India

We investigate the structure and activated dynamics of a binary mixture of colloidal particles dispersed in a solvent of much smaller-sized particles. The solvent degrees of freedom are traced out from the grand partition function of the colloid-solvent mixture which reduces the system from ternary to effective binary mixture of colloidal particles. In the effective binary mixture colloidal particles interact via effective potential that consists of bare potential plus the solvent-induced interaction. Expressions for the effective potentials and pair correlation functions are derived. We used the result of pair correlation functions to determine the number of particles in a cooperatively reorganizing cluster (CRC) in which localized particles form "long-lived" nonchemical bonds with the central particle. For an event of relaxation to take place these bonds have to reorganize irreversibly, the energy involved in the processes is the effective activation energy of relaxation. Results are reported for hard sphere colloidal particles dispersed in a solvent of hard sphere particles. Our results show that the concentration of solvent can be used as a control parameter to fine-tune the microscopic structural ordering and the size of CRC that governs the glassy dynamics. We show that a small variation in the concentration of solvent creates a bigger change in the kinetic fragility which highlights a wide variation in behavior, ranging from fragile to strong glasses. We conclude that the CRC which is determined from the static pair correlation function and the fluctuations embedded in the system is probably the sole player in the physics of glass transition.

I. INTRODUCTION

Hard spheres which interact only as a result of excluded volumes have extensively been used to model liquids, glasses, crystals, colloidal systems, granular materials, etc. Random packing of hard spheres is a subject of wide interest as they are linked to important mathematical problems of signal digitalization, error-correcting codes, and optimization problems [1]. Experimentally hard sphere systems are realized using colloidal particles, emulsions, and granular particles [2–4]. For several decades, attempts have been made to find a way to characterization of amorphous packing, glass transition, and the nature of random close packings (RCP) [1–13].

In a one-component system of hard spheres, the fluid-crystal transition takes place at packing fraction $\eta = 0.494$ and the melting transition at $\eta = 0.545$. But when the system is compressed following a protocol that avoids crystallization, the compressed fluid starts above $\eta \simeq 0.53$ to attain solidlike behavior marked by a rapid increase of structural relaxation time (or viscosity) and eventually falls out of equilibrium at the glass transition $\eta_g \simeq 0.58$ where particle crowding greatly restricts relaxation [14–18]. However, a system of monodisperse hard spheres is a poor glass former as it crystallizes easily [19,20]. This crystallization propensity is usually prevented by introducing polydispersity [21–23] or by adding a second component with different-sized hard spheres. In a mixture, amorphous packing and glass transition depends on particle size ratio $q = \sigma_b/\sigma_a$ and mixing ratio $x_b = \eta_b/(\eta_a + \eta_b)$ [23–29]. Here and below symbols a and b denote particles

of species of larger and smaller-sized spheres with diameters σ_a and σ_b, respectively. Experiment and simulation results show that for moderate values of $q \gtrsim 0.35$ the glass transition shifts to a larger total packing fractions $\eta(= \eta_a + \eta_b)$ at intermediate compositions compared to a monocomponent system. This behavior is similar to the one found for moderately polydisperse systems [21–23] On the other hand, for $q \lesssim 0.35$ different glass states distinguished by the arrest mechanism of large spheres and the mobility of small spheres are reported [23–34].

The dramatic rise of the structural relaxation time τ_α (or viscosity) in a narrow temperature or density range near the glass transition is a characteristic feature of fragile glass formers. In the case of molecular (thermal) liquids, a wide variation in the behavior of τ_α near the glass transition temperature T_g is observed [35,36]. This becomes evident in a renormalized Arrhenius plot where temperature T is rescaled by T_g. This observed behavior is characterized by the unifying concept of fragility. For molecular glass formers, the fragility is defined by the logarithmic slope of τ_α at T_g [35,36] which highlights the wide variation ranging from strong to fragile and provides a unifying conceptual framework. Since in the case of hard spheres temperature becomes irrelevant, the fragility has to be defined by the logarithmic slope of τ_α at the glass transition packing fraction η_g [37,38]. This restricts the fragile behavior of hard spheres glass formers and, therefore, their versatility as a model system of the glass transition. However, when soft colloidal particles are examined at fixed T by varying η, the fragility shows the same behavior as in the T dependence of

molecular liquids at fixed η; variations of T and η give a broad spectrum of fragility [39–41]. Polydispersity is also found to affect the fragility [42].

In this paper, we investigate size asymmetric ternary mixtures of hard spheres and calculate τ_α and fragility at different concentrations of the species of smallest-sized particles of the mixture dubbed as a solvent. In particular, the mixture we investigate consists of hard spheres of diameters $\sigma_a = 1.4$, $\sigma_b = 1.0$, and $\sigma_s = 0.28$; particles size ratios are $q_{ab} = 0.714$, $q_{as} = 0.2$, and $q_{bs} = 0.28$. We call species a, b, and s as a solute, cosolute, and solvent, respectively. Whenever needed we call a and b particles collectively as colloid particles and denote them by symbol c. The system is characterized by packing fractions $\eta_a = \frac{\pi}{6}\rho_a\sigma_a^3$, $\eta_b = \frac{\pi}{6}\rho_b\sigma_b^3$, and $\eta_s = \frac{\pi}{6}\rho_s\sigma_s^3$ where $\rho_a = N_a/V$, $\rho_b = N_b/V$, and $\rho_s = N_s/V$. Here V is the volume, and N_α is the ensemble-averaged number of particles of species α. A binary mixture of species a and b with $\rho_a = \rho_b$ has been studied using the Monte Carlo algorithm by Berthier and Witten [43] and Brambilla *et al.* [18]. In order to compare our results for a binary mixture of species a and b (i.e., for $\eta_s = 0$) with those of Refs. [18,43] we choose $\rho_a = \rho_b$. Thus, the system is characterized by two independent variables $\eta_c = \eta_a + \eta_b$ and η_s with total packing fraction $\eta = \eta_c + \eta_s$.

In Sec. II we give a brief description of a theory developed in Refs. [44–46] for calculating the activation energy barrier of relaxation and τ_α. The theory identifies the local structural order that defines the cooperativity of relaxation. In a supercompressed (supercooled) fluid some particles get trapped in potential wells (cages) created by neighbors and form long-lived (stable) nonchemical bonds between them. For an event of structural relaxation to take place, the cluster has to reorganize irreversibly. The number of particles in the cluster defines the size of cooperativity. The number of particles that forms the cluster and the activation energy barrier of relaxation is calculated from data of pair correlation functions.

Pair correlation functions are usually calculated using integral equation theory (IET) or computer simulations. The IET consists of the Ornstein-Zernike (OZ) equation and the so-called closure relation. However, tackling highly asymmetric mixtures via multicomponent OZ equation where all species are treated on equal footing is extremely difficult [47–49]. As for as simulation is concerned, the required computational investment for asymmetry mixtures is generally prohibitive because of the very slow relaxation of big particles caused by smaller particles [50,51]. To avoid the complexity arising due to large size asymmetry one prefers coarse graining (CG), i.e., trace out solvent degrees of freedom. This reduces the system to an effective binary mixture of species a and b with modest size asymmetry. In the effective binary mixtures, particles interact via potentials which are a combination of bare (direct) interaction and solvent-induced interaction (SII). In Sec. III we summarize a theory developed in Refs. [52,53] to trace out solvent degrees of freedom and derive an expression for the effective potential and correlation functions. Note that the theories described in Secs. II and III are equally valid to thermal (molecular) and athermal systems. In Sec. IV we calculate the number of particles in the cooperatively reorganizing cluster (CRC), τ_α, and the fragility as a function of η_s and present results for systems of hard spheres. The paper ends with a summary and conclusions described in Sec. V.
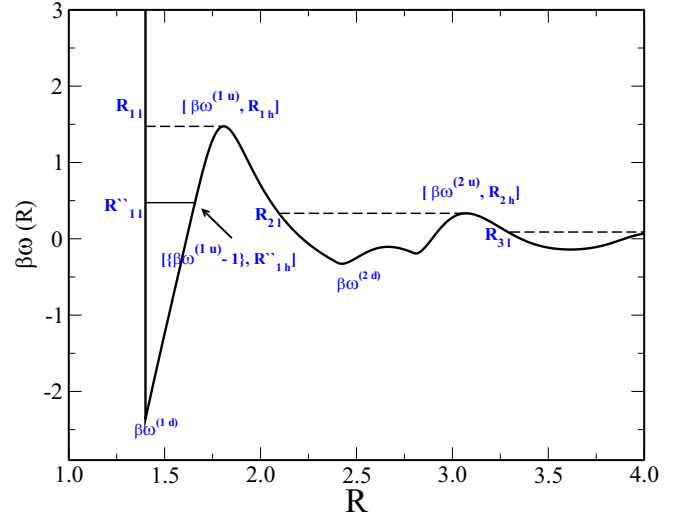

FIG. 1. Plot of potential (potential of mean force) $\beta w_{\alpha\gamma}(R)$ between a pair of particles of species α and γ separated by distance R (expressed in units of σ_{bb}) in a system of hard spheres. $\beta w^{(iu)}$ and R_{ih} are, respectively, value and location of ith maximum and R_{il} is the location on the left-hand side of the shell where $\beta w^{(i)}(R) = \beta w^{(iu)}$ (shown by the dashed line). The location R''_{il} and R''_{ih} are values of R on the left- and the right-hand sides of the shell where $\beta w^{(i)}(R) = [\beta w^{(iu)} - 1]$ (shown by the full line). $\beta w^{(id)}$ is the depth of the ith shell.

II. COOPERATIVELY REORGANIZING CLUSTER, ACTIVATION ENERGY AND THE RELAXATION TIME τ_α

The theory developed in Refs. [44–46] provides a method to distinguish and calculate a number of dynamically free, metastable, and stable (long-lived) neighbors of a tagged (central) particle in a system as a function of T and η. This is achieved by including momentum distribution in the definition of the correlation function $g_{\alpha\gamma}(R)$. Thus,

$$g_{\alpha\gamma}(R) = \left(\frac{\beta}{2\pi\mu}\right)^{3/2} \int d\mathbf{p}\, e^{-\beta[(p^2/2\mu)+w_{\alpha\gamma}(R)]}. \quad (2.1)$$

where $\mathbf{p}$ is the relative momentum of a particle of mass μ and $\beta w_{\alpha\gamma}(R) = -\ln g_{\alpha\gamma}(R)$ is the potential of mean force (reduced potential) [53] between a pair of particles α and γ ($\alpha, \gamma \in [a, b]$) separated by distance R in the mixture. In writing the above equation we assumed particles of species a and b have equal mass and identical Maxwell-Boltzmann distribution of momentum p. The peaks and troughs of $g_{\alpha\gamma}(R)$ create, respectively, minima and maxima in $\beta w_{\alpha\gamma}(R)$ as shown in Fig. 1. In the figure a region between two maxima, leveled as $i - 1$ and i ($i \geqslant 1$) is denoted as the ith shell and the minimum of the shell as $\beta w^{(id)}_{\alpha\gamma}$. The value of the ith maximum (barrier) is denoted as $\beta w^{(iu)}_{\alpha\gamma}$, and its location is denoted by R_{ih}.

In a classical system, all those particles whose energies are less or equal to $\beta w^{(iu)}_{\alpha\gamma}$ would be trapped in the ith shell as they do not have enough energy to escape the barrier, and all those particles whose energies are higher than $\beta w^{(iu)}_{\alpha\gamma}$ are free to move around. The number of trapped particles that can be considered to be bonded (nonchemical) with the central

particle is found to form a part of $g_{\alpha\gamma}(R)$ defined as [44–46]

$$
g_{\alpha\gamma}^{(ib)}(R) = 4\pi \left(\frac{\beta}{2\pi\mu} \right)^{3/2} e^{-\beta w_{\alpha\gamma}^{(i)}(R)}
$$
$$
\times \int_0^{\sqrt{2\mu[w_{\alpha\gamma}^{(iu)}-w_{\alpha\gamma}^{(i)}(R)]}} e^{-\beta p^2/2\mu} p^2 \, dp, \quad (2.2)
$$

where $w_{\alpha\gamma}^{(i)}(R)$ is the potential in the range of $R_{il} \leqslant R \leqslant R_{ih}$ of the ith shell. Here R_{il} is the value of R where $w_{\alpha\gamma}^{(i)}(R) = w_{\alpha\gamma}^{(iu)}$ on the left-hand side of the shell (see Fig. 1). The total number of particles that form bonds with the central particle of species α is

$$
n_\alpha^{(b)} = 4\pi \sum_i \sum_\gamma \rho_\gamma \int_{R_{il}}^{R_{ih}} g_{\alpha\gamma}^{(ib)}(R) R^2 \, dR, \qquad (2.3)
$$

where summations are over all shells and over all species and ρ_γ is the number density of the γ component. The number $n_\alpha^{(b)}$ increases rapidly as η is increased. However, fluctuations embedded in the system (bath) activate some of these bonded particles to escape the barrier. These particles are referred to as metastable (or m) particles. The remaining bonded particles stay trapped in shells and form stable bonds with the central particle and are referred to as l particles. In the case of hard spheres, all those particles whose energies lie between $\beta w_{\alpha\gamma}^{(iu)} - 1$ and $\beta w_{\alpha\gamma}^{(iu)}$ are m particles [44]. All those particles whose energies are between $\beta w_{\alpha\gamma}^{(id)}$ and $[\beta w_{\alpha\gamma}^{(iu)} - 1]$ are l particles. The number of l particles is found from a part of $g_{\alpha\gamma}(R)$ defined as

$$
g_{\alpha\gamma}^{(il)}(R) = 4\pi \left(\frac{\beta}{2\pi\mu} \right)^{3/2} e^{-\beta w_{\alpha\gamma}^{(i)}(R)}
$$
$$
\times \int_0^{\sqrt{2\mu[w_{\alpha\gamma}^{(iu)}-k_BT-w_{\alpha\gamma}^{(i)}(R)]}} e^{-\beta p^2/2\mu} p^2 \, dp, \quad (2.4)
$$

where $w_{\alpha\gamma}^{(i)}(R)$ is in the range of $R_{il}'' \leqslant R \leqslant R_{ih}''$. Here R_{il}'' and R_{ih}'' are, respectively, the value of R on the left- and the right-hand sides of the shell where $\beta w_{\alpha\gamma}^{(i)}(R) = \beta w_{\alpha\gamma}^{(iu)} - 1$. The number of l particles around an α particle is

$$
n_\alpha^{(l)} = 4\pi \sum_i \sum_\gamma \rho_\gamma \int_{R_{il}''}^{R_{ih}''} g_{\alpha\gamma}^{(il)}(R) R^2 \, dR. \qquad (2.5)
$$

The averaged number of l particles bonded with a central particle in a binary mixture is

$$
n^{(l)} = x_a n_a^{(l)} + x_b n_b^{(l)}, \qquad (2.6)
$$

where x_α is the concentration of species α. The cluster of $n^{(l)} + 1$, particles form a CRC. The effective activation energy of relaxation is given as

$$
\beta E^{(l)}(\eta) = 4\pi \sum_i \sum_\gamma x_\gamma \rho_\gamma \int_{R_{il}''}^{R_{ih}''} \left[\beta w_{\alpha\gamma}^{(iu)} - 1 - \beta w_{\alpha\gamma}^{(i)}(R) \right]
$$
$$
\times g_{\alpha\gamma}^{(il)}(R) R^2 \, dR, \qquad (2.7)
$$

where energy is measured from the effective barrier $\beta w_{\alpha\gamma}^{(iu)} - 1$. The structural relaxation time τ_α is obtained from the Arrhenius law,

$$
\tau_\alpha(\eta) = \tau_0 \exp[\beta E^{(l)}(\eta)], \qquad (2.8)
$$

where τ_0 is a microscopic timescale.

The only input we need to calculate τ_α is the values of $g_{\alpha\gamma}(R)$ at different values of η_c and η_s. In the following section, we describe a method used to coarse grain the system and derive equations which are used to calculate values of $g_{\alpha\gamma}(R)$.

III. THEORY TO TRACE OUT THE SOLVENT DEGREES OF FREEDOM AND REDUCTION OF THE SYSTEM TO AN EFFECTIVE BINARY MIXTURE OF COLLOIDAL PARTICLES

When one traces out all variables belonging to solvent particles from the system partition function, one ends up with a coarse-grained partition function of the surviving components. If the coarse graining is performed exactly, the coarse-grained partition functions account exactly for the effect of the degrees of freedom that have been subsumed. Thus, the structural and thermodynamic properties of colloidal components of the mixture will be identical in both the coarse-grained and the full-system description.

The grand partition function of the ternary mixture is written as

$$
\Xi(\mu_a, \mu_b, V, T) = \sum_{N_a \geqslant 0} \sum_{N_b \geqslant 0} \mathrm{Tr}_a \mathrm{Tr}_b \exp(\beta(\mu_a + \mu_b)
$$
$$
- W_s[\vec{R}_a, \vec{R}_b] - \beta H_{aa}\{\vec{R}_a^{N_a}\}
$$
$$
- \beta H_{bb}\{\vec{R}_b^{N_b}\} - \beta H_{ab}\{\vec{R}_a^{N_a}, \vec{R}_b^{N_b}\}), \quad (3.1)
$$

where

$$
e^{W_s[\vec{R}_a, \vec{R}_b]} = \sum_{N_s \geqslant 0} \mathrm{Tr}_s \exp\left(\beta\mu_s N_s - \beta U_{ss}\{\vec{R}_s^{N_s}\} \right.
$$
$$
\left. - \beta \sum_\alpha H_{\alpha s}\{\vec{R}_\alpha^{N_\alpha}, \vec{r}^{N_s}\} \right). \qquad (3.2)
$$

In (3.1) and (3.2), Tr_α stands for $\frac{1}{N_\alpha! \Lambda^{3N_\alpha}} \int_V d\vec{R}^{N_\alpha}$, Λ is the thermal wavelength, μ_α is the chemical potential, N_α is number of particles of species α in volume V. $\beta = (k_B T)^{-1}$ is the inverse temperature in units of the Boltzmann constant k_B, $\vec{R}_a$, $\vec{R}_b$, and $\vec{r}$ are the position vectors of particles of species a, b, and s, respectively. $H_{\alpha\gamma}$ represents the interaction potential between particles of similar and different species. $W_s[\vec{R}_a, \vec{R}_b]$ is the grand thermodynamics potential of the solvent in the presence of solute and cosolute particles that exert "external" potential field on solvent particles.

Since position vectors of a and b particles are held fixed when integration over s particles is performed, W_s depends on the constrained position vectors of solute and co-solute particles. This fact is emphasized by the square bracket. The constrained spatial configurations of a and b particles can be described in terms of single particle density operators defined as

$$
\hat{\rho}_a(\vec{R}_a) = \sum_{i=1}^{N_a} \delta(\vec{R}_a - \vec{R}_{ai}) \quad \text{and} \quad \hat{\rho}_b(\vec{R}_b) = \sum_{i=1}^{N_b} \delta(\vec{R}_b - \vec{R}_{bi}),
$$
$$
(3.3)
$$

where δ is the Dirac function. The potential field that acts on a tagged s particle at position $\vec{r}$ due to a and b particles is as

follows:

$$\phi_s(\vec{r}) = \sum_\alpha \sum_{i=1}^{N_\alpha} u_{\alpha s}(|\vec{R}_{\alpha i} - \vec{r}|), \tag{3.4}$$

where α stands for a and b and $u_{\alpha s}$ is the pair potential between particles of species α and s. The above relation is used to rewrite (3.2) as

$$e^{W_s[\vec{R}_a, \vec{R}_b]} = \sum_{N_s \geqslant 0} \mathrm{Tr}_s \exp\left(\sum_{i=1}^{N_s} \psi(\vec{r}_i) - \beta \sum_{i<j} u_{ss}(|\vec{r}_i - \vec{r}_j|) \right), \tag{3.5}$$

where $\psi(\vec{r}) = \beta[\mu_s - \phi_s(\vec{r})]$ is the *reduced intrinsic chemical potential* [55] which acts as a field variable conjugate to single particle density $\rho_s(\vec{r})$.

Since $W_s[\vec{R}]$ is a local functional of $\psi_s(\vec{r})$ [55] its functional derivatives with respect to $\psi_s(\vec{r})$ taken at constant T give

$$\frac{\delta W_s[\vec{R}_a, \vec{R}_b]}{\delta \psi(\vec{r}_1)} = \rho_s(\vec{r}_1), \tag{3.6}$$

and

$$\begin{aligned}
\frac{\delta^2 W_s[\vec{R}_a, \vec{R}_b]}{\delta \psi(\vec{r}_1)\delta \psi(\vec{r}_2)} &= \rho_s^{(2)}(\vec{r}_1, \vec{r}_2) - \rho_s(\vec{r}_1)\rho_s(\vec{r}_2) \\
&\quad + \rho_s(\vec{r}_1)\delta(|\vec{r}_1 - \vec{r}_2|) \\
&= \chi_{ss}(\vec{r}_1, \vec{r}_2).
\end{aligned} \tag{3.7}$$

Here $\rho_s(\vec{r})$ and $\rho_s^{(2)}(\vec{r}_1, \vec{r}_2)$ are the ensemble-averaged one- and two-body density, and χ_{ss} is the density-density correlation function of the solvent [56]. When functional integrals of (3.6) and (3.7) are performed along a linear integration path between the reference (pure solvent) and the final state (full mixture) such that $\psi_{s,\lambda}(\vec{r}) = \beta\mu_s + \lambda\Delta\psi_s(\vec{r})$, where $\Delta\psi_s(\vec{r}) = \psi_s(\vec{r}) - \beta\mu_s$, one gets

$$\delta\rho_s(\vec{r}_1) = \rho_s(\vec{r}_1) - \rho_s = \int d\vec{r}_2 \tilde{\chi}_{ss}(\vec{r}_1, \vec{r}_2)\Delta\psi_s(\vec{r}_2), \tag{3.8}$$

and

$$\begin{aligned}
W_s[\vec{R}_a, \vec{R}_b] - W_s^{(0)} &= \rho_s \int d\vec{r}_1 \Delta\psi_s(\vec{r}_1) - \frac{1}{2}\int d\vec{r}_1 \\
&\quad \times \int d\vec{r}_2 \Delta\psi_s(\vec{r}_1)\bar{\chi}_{ss}(\vec{r}_1, \vec{r}_2)\Delta\psi_s(\vec{r}_2),
\end{aligned} \tag{3.9}$$

where

$$\tilde{\chi}_{ss}(\vec{r}_1, \vec{r}_2) = \int_0^1 d\lambda \chi_{ss}(\vec{r}_1, \vec{r}_2; \lambda), \tag{3.10}$$

and

$$\bar{\chi}_{ss}(\vec{r}_1, \vec{r}_2) = 2\int_0^1 d\lambda(1-\lambda)\chi_{ss}(\vec{r}_1, \vec{r}_2; \lambda). \tag{3.11}$$

The field $\Delta\psi_s(\vec{r})$ can be defined in terms of a functional that couples the solvent to the solute and the cosolute density fields as [53]

$$\frac{\delta\Delta\psi_s(\vec{r})}{\delta\rho_\alpha(\vec{R}_\alpha)} = c_{\alpha s}(\vec{r}, \vec{R}_\alpha). \tag{3.12}$$

The functional integration of (3.12) gives

$$\Delta\psi_s(\vec{r}) = \sum_\alpha \int_0^1 d\lambda \int d\vec{R}_\alpha c_{\alpha s}(\vec{r}, \vec{R}_\alpha; \lambda)\hat{\rho}_\alpha(\vec{R}_\alpha) \tag{3.13}$$

$$= \sum_\alpha \sum_i^{N_\alpha} \bar{c}_{\alpha s}(\vec{r}, \vec{R}_{\alpha,i}), \tag{3.14}$$

where

$$\bar{c}_{\alpha s}(\vec{r}, \vec{R}_{\alpha,i}) = \int_0^1 d\xi \, c_{\alpha s}(\vec{r}, \vec{R}_\alpha; \xi). \tag{3.15}$$

Here ξ acts as a **charging parameter** that raises the solute and cosolute potential fields that act on the solvent particle from zero to their full value as it varies from 0 to 1. Combining (3.9) and (3.14) we get

$$\begin{aligned}
W_s[\vec{R}_a, \vec{R}_b] &= W_s^{(0)} - \sum_\alpha \sum_{i=1}^{N_\alpha} \phi_\alpha(\vec{R}_{\alpha i}) \\
&\quad - \frac{1}{2}\sum_{i\neq j}^{N_s} \sum_\alpha^{N_\alpha} \sum_\gamma^{N_\gamma} v_{\alpha,\gamma}(\vec{R}_{\alpha i}, \vec{R}_{\gamma j}),
\end{aligned} \tag{3.16}$$

where

$$\begin{aligned}
\phi_\alpha(\vec{R}_{\alpha i}) &= -\int d\vec{r}_1 c_{\alpha s}(\vec{r}_1, \vec{R}_{\alpha,i}) \\
&\quad \times \left[\rho_s + \frac{1}{2}\int d\vec{r}_2 \bar{\chi}_{ss}(\vec{r}_1, \vec{r}_2)c_{\gamma s}(\vec{r}_2, \vec{R}_{\gamma,i}) \right],
\end{aligned} \tag{3.17}$$

and

$$\begin{aligned}
v_{\alpha\gamma}(\vec{R}_{\alpha i}, \vec{R}_{\gamma j}) &= -\int d\vec{r}_1 \int d\vec{r}_2 \bar{c}_{\alpha s}(\vec{r}_1, \vec{R}_{\alpha,i}) \\
&\quad \times \bar{\chi}_{ss}(\vec{r}_1, \vec{r}_2)\bar{c}_{\gamma s}(\vec{r}_2, \vec{R}_{\gamma,i}).
\end{aligned} \tag{3.18}$$

Here $\alpha, \gamma \in [a, b]$, $\phi_\alpha(\vec{R}_\alpha)$ is the solvent-induced potential field acting on an α particle at $\vec{R}_\alpha$ and $v_{\alpha\gamma}(\vec{R}_{\alpha i}, \vec{R}_{\gamma j})$ is the SII between α and γ particles.

From (3.1) and (3.16) we now have

$$\Xi(\mu_a, \mu_b, \mu_c, V, T) = e^{W_s^{(0)}}\Xi_c(\mu_a, \mu_b, V, T), \tag{3.19}$$

where

$$\begin{aligned}
&\Xi_c(\mu_a, \mu_b, V, T) \\
&= \sum_{N_a \geqslant 0}\sum_{N_b \geqslant 0} \mathrm{Tr}_a\mathrm{Tr}_b \exp\left(\beta\sum_\alpha \sum_{i=1}^{N_\alpha} \psi_\alpha(\vec{R}_{\alpha i}) \right. \\
&\quad - \frac{1}{2}\beta\sum_{i\neq j}^{N_a} U_{aa}(\vec{R}_{ai}, \vec{R}_{aj}) - \frac{1}{2}\beta\sum_{i\neq j}^{N_b} U_{bb}(\vec{R}_{bi}, \vec{R}_{bj}) \\
&\quad \left. - \beta\sum_{i=j}^{N_a}\sum_{i=j}^{N_b} U_{ab}(\vec{R}_{ai}, \vec{R}_{bj}) \right).
\end{aligned} \tag{3.20}$$

Here

$$\psi_\alpha(\vec{R}_{\alpha i}) = \beta[\mu_\alpha - k_B T \phi_\alpha(\vec{R}_{\alpha i})], \tag{3.21}$$

and

$$U_{\alpha\gamma}(\vec{R}_{\alpha i}, \vec{R}_{\gamma j}) = u_{\alpha\gamma}(|\vec{R}_{\alpha i} - \vec{R}_{\alpha j}|) + k_B T v_{\alpha\gamma}(\vec{R}_{\alpha i}, \vec{R}_{\gamma j}). \tag{3.22}$$

Equation (3.20) defines the CG grand partition functions of a binary mixture of solute and cosolute particles in volume V and temperature T.

The function $\bar{c}_{\alpha s}$ is determined from a relation given as [52,53]

$$\rho_s h_{\alpha s}(|\vec{r} - \vec{R}_{\alpha i}|)$$
$$= \rho_s + \sum_\gamma \int d\vec{r}' \widetilde{\chi}_{ss}(\vec{r}, \vec{r}') \bar{c}_{\gamma s}(\vec{r}') + \sum_\gamma \sum_j (1 - \delta_{ij})$$
$$\times \int d\vec{r}' \widetilde{\chi}_{ss}(\vec{r}, \vec{r}') \bar{c}_{\gamma s}(\vec{r}', \vec{R}_{\gamma j}), \tag{3.23}$$

where distances are measured from a colloidal particle of species α fixed at $\vec{R}_{\alpha i}$. This relation is found from functional derivatives of ΔW with respect to $c_{\alpha s}(\vec{r}, \vec{R}_{\alpha i})$ or from (3.8). Note that all relations given above and expressed in terms of functionals $\bar{c}_{\alpha s}$ and $\bar{\chi}_{ss}$ are exact. However, they correspond to constrained configurations of colloidal particles. As argued in Refs. [52,53] we can simplify these expressions by replacing the constrained configurations by the most probable configurations determined by the configurational probability density defined in terms of the Boltzmann factor of the CG Hamiltonian of the effective binary mixture. This allows us to rewrite (3.23) as (see Ref. [53])

$$\rho_s h_{\alpha s}(r) = \sum_\gamma \left[\int d\vec{r}' \widetilde{\chi}_{ss}(\vec{r}, \vec{r}') \bar{c}_{\gamma s}(\vec{r}') \right.$$
$$\left. + \int d\vec{r}' \int d\vec{R}_\gamma \, \widetilde{\chi}_{ss}(\vec{r}, \vec{r}') \bar{c}_{\gamma s}(\vec{r}', \vec{R}_\gamma) h_{\alpha\gamma}(\vec{R}_\alpha, \vec{R}_\gamma) \right]. \tag{3.24}$$

Solution of (3.24) gives $\bar{c}_{\alpha s}$ which is used to find potential $v_{\alpha\gamma}(R)$ from (3.18). From known effective interaction $U_{\alpha\gamma}$ one calculates $h_{\alpha\gamma}(R)$ and $g_{\alpha\gamma}(R)$ using the one component OZ equation with a closure relation.

IV. RESULTS

A. Pair correlation function $g_{\alpha\gamma}(R)$ and number of particles in a cooperatively reorganizing cluster

We use a numerical procedure developed in Ref. [53] and summarized in the Appendix to calculate the effective potential $U_{\alpha\gamma}(R)$, and correlation function $g_{\alpha\gamma}(R)$ for the effective binary mixture at different values of η_s. When $\eta_s = 0$, the system, as stated above reduces to a binary mixture of colloidal particles interacting via pair potential $u_{\alpha\gamma}(R)$. We use the mixture OZ equation and the thermodynamically self-consistent closure relation of Rogers and Young [57] to calculate pair correlation function $g_{\alpha\gamma}^{(bm)}(R)$. Here superscript bm is used to indicate that the results correspond to the colloidal mixture when $\eta_s = 0$. In Fig. 2(a) we compare calculated values of $g^{(bm)}(R)$ defined as

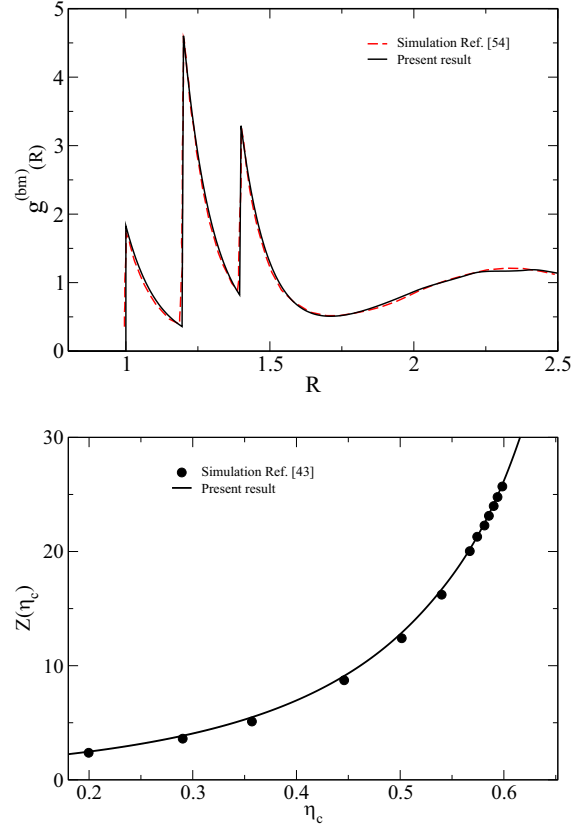$$g^{(bm)}(R) = x_a^2 g_{aa}^{(bm)}(R) + 2x_a x_b g_{ab}^{(bm)}(R) + x_b^2 g_{bb}^{(bm)}(R), \quad (4.1)$$

FIG. 2. (a) Comparison of calculated values of pair correlation function $g_{\alpha\gamma}^{(bm)}(R)$ at packing fraction $\eta_c = 0.58$ with the Monte Carlo simulation values [54]. R is expressed in units of σ_{bb}. The three peaks correspond to the separation at contact for the binary mixture. (b) Comparison of calculated values of equilibrium pressure with the Monte Carlo simulation values [43]. The agreement between the values is very good over the entire range of η_c shown in the figure.

with simulation values reported by Callaham and Machta [54] for $\eta_c = 0.58$ and in Fig. 2(b) values of $Z(\eta_c) = \frac{\beta P_c}{\rho_c}$ (P_c is the pressure) with simulation values given in Ref. [43]. We note that the calculated values of correlation function and pressure are in excellent agreement with simulation values. When η_s is nonzero we use an iterative method in which $g_{\alpha\gamma}(R)$ is calculated using the hypernetted chain (HNC) and reference hypernetted chain (RHNC) closure relation where $g_{\alpha\gamma}^{(bm)}(R)$ appears as a reference term [see Eq. (A7)].

In Figs. 3–6, we plot values of $\beta U_{\alpha\gamma}(R)$ and $g_{\alpha\gamma}(R)$ for several values of η_c at solvent packing fraction $\eta_s = 0.1$ and $\eta_s = 0.2$. These figures give a quantitative measure of the solvent-induced effective potential between colloidal particles and their distributions in the solvent. In all the cases $\beta U_{\alpha\gamma}(R)$ is attractive at contact and rises to form a repulsive peak at $R \sim \sigma_{\alpha\gamma} + \frac{1}{2}q_{bs}$; $\frac{1}{2}q_{bs}$ is the radius of a solvent particle. All lengths are expressed in units of σ_{bb}. This attraction is attributed to the depletion region formed between colloidal particles when their separation is less than the radius of the solvent particle. Due to the depletion, a pressure gradient originates giving rise to a short-range entropy-driven attractive effective potential; the depletion potential. Depending on values of η_s and η_c, $\beta U_{\alpha\gamma}(R)$ may form a few more minima and maxima before
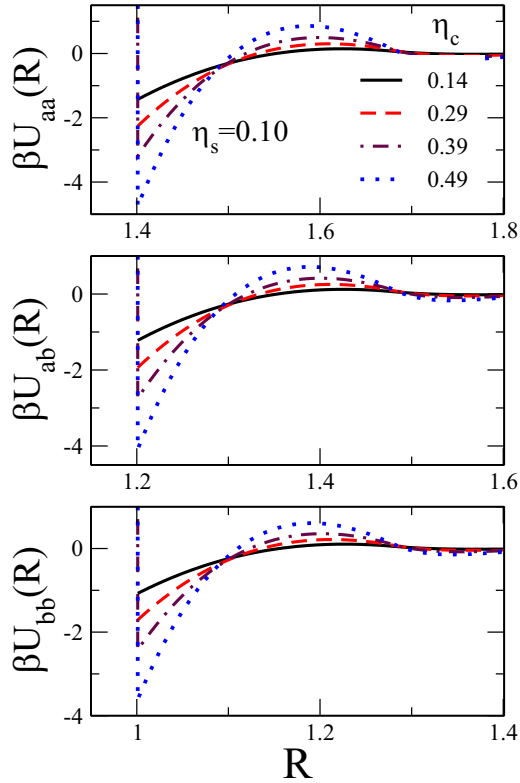
FIG. 3. Effective potential $\beta U_{\alpha\gamma}(R)$ between a pair of solute and cosolute (colloidal) particles separated by distance R (measured in units of σ_{bb}) at solvent packing fraction $\eta_s = 0.1$ for several values of η_c.

FIG. 4. Pair distribution function $g_{\alpha\gamma}(R)$ of colloidal particles vs R (measured in units of σ_{bb}) at $\eta_s = 0.1$ for several values of η_c.

decaying to zero. The minima occur at preferential distances allowing for an integer number of layers of solvent particles between colloidal particles. Repulsion arises when solvent particles move to disturb these layers of solvent particles. The minimum at $R \sim \sigma_{\alpha\gamma} + q_{bs}$ in $\beta U_{\alpha\gamma}(R)$ corresponds to the configuration when one layer of solvent particles is sandwiched between two colloidal particles. These features of $\beta U_{\alpha\gamma}(R)$ are reflected in the nature of $g_{\alpha\gamma}(R)$ which gives information about the distribution of colloidal particles. In $g_{\alpha\gamma}(R)$ a deep minimum appears at $R \sim \sigma_{\alpha\gamma} + \frac{1}{2}q_{bs}$ which separates a pronounced peak of $R \sim \sigma_{\alpha\gamma}$ and a relatively weak peak at $R \sim \sigma_{\alpha\gamma} + q_{bs}$ where a minimum of $\beta U_{\alpha\gamma}(R)$ occurs. Maxima and minima of $g_{\alpha\gamma}(R)$ become more pronounced on increasing η_s. In Fig. 7 we compare $g_{aa}(R)$ found for $\eta = 0.59$ and $\eta_s = 0.0, 0.1$ and 0.2 to show the change that takes place in the distribution of colloidal particles on increasing concentration of solvent particles. Due to this change in $g_{\alpha\gamma}(R)$ the potential well $\beta w_{\alpha\gamma}(R)$ changes on changing η_s and which, in turn, changes the number of particles in CRC. We plot in Figs. 8–10 $\beta w_{\alpha\gamma}(R)$ for $\eta_s = 0.0, 0.1,$ and 0.2 and for each case several values of η_c. To compare the effect of solvent concentration on the potential well we compare $\beta w_{aa}(R)$ for the three values of η_s in Fig. 11(a) for $\eta = 0.59$ and in Fig. 11(b) for $\eta_c = 0.39$. The most noticeable change that takes place in $\beta w_{\alpha\gamma}(R)$ due to solvent particles is a change in the width of the potential well. Although the maximum and minimum of the first shell where most l particles appear have increased,
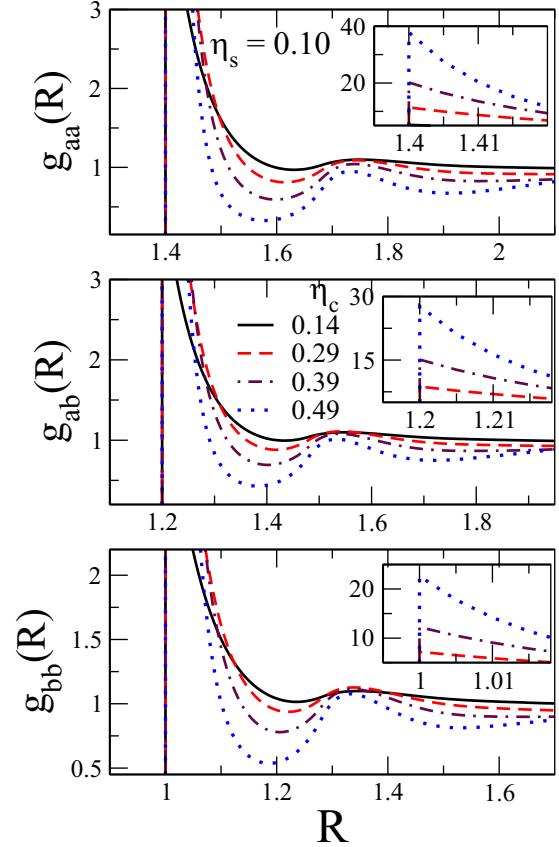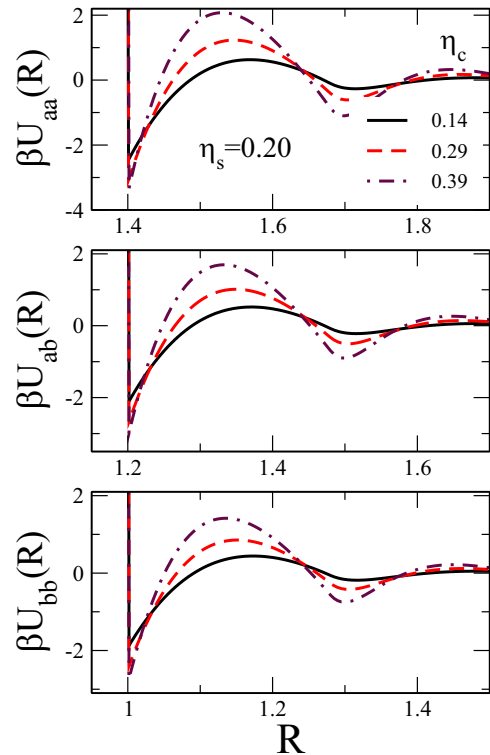

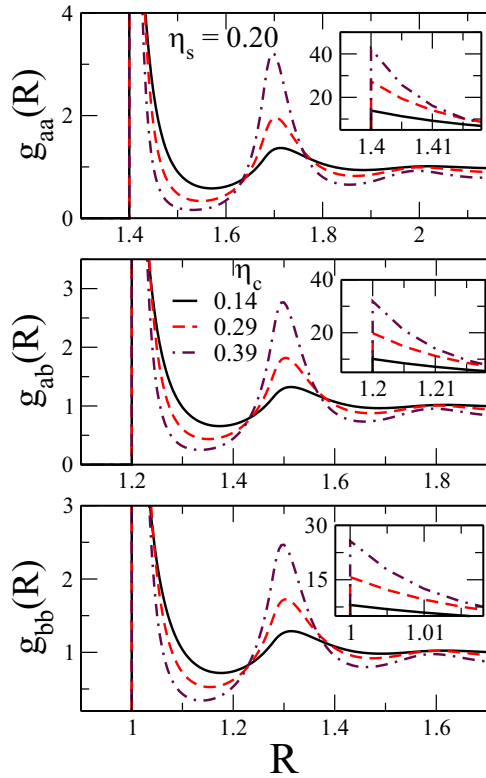FIG. 5. The same as for Fig. 3 but with $\eta_s = 0.2$.

FIG. 6. The same as for Fig. 4 but with $\eta_s = 0.2$.

but the width has narrowed. As a consequence, the number of long-lived particles that form CRC change with η_s.

In Figs. 12–14 we plot $g^{(l)}_{\alpha\gamma}(R)$ vs R, respectively, for $\eta_s = 0.0, 0.1,$ and 0.2. For each case, results are given for several values of η_c to show how $g^{(l)}_{\alpha\gamma}(R)$ depends on colloidal and solvent packing fractions. The number of particles $n^{(l)}$ that form CRC is plotted in Fig. 15(a) as a function of η_c and in
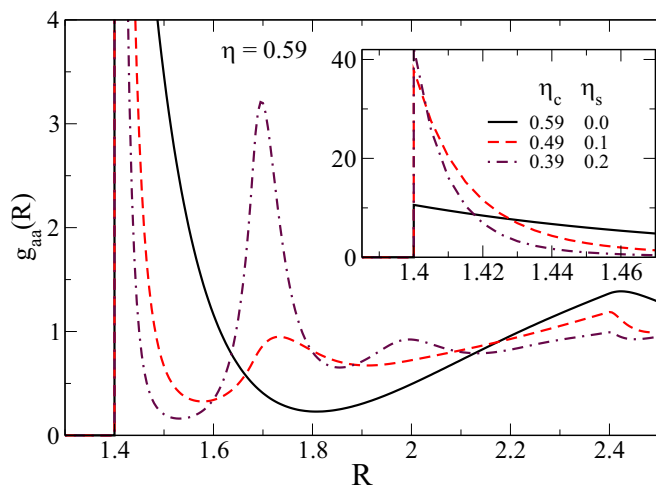
FIG. 7. Comparison of values of pair distribution function $g_{aa}(R)$ as a function of R (measured in units of σ_{bb}) for total packing fraction $\eta = 0.59$ and solvent packing fractions $\eta_s = 0.0, 0.1$ and 0.2 to show the change that takes place in the distribution of colloidal particles of species a on increasing concentration of solvent particles. Similar results are also found for species b.
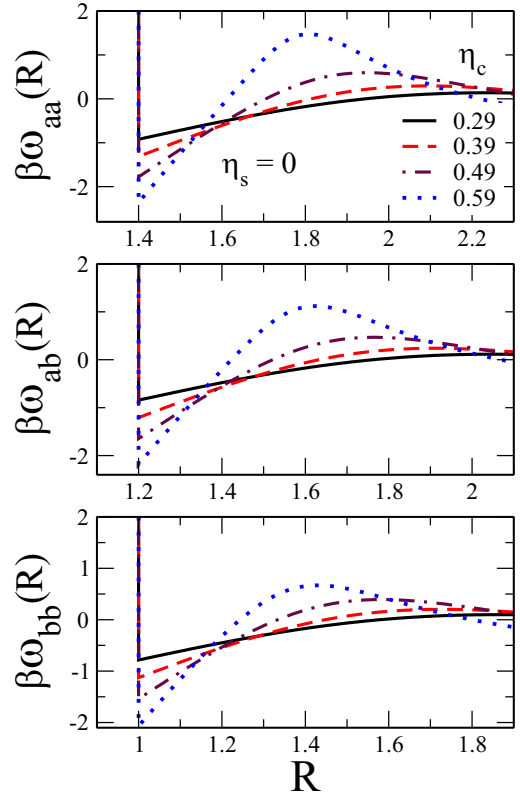

FIG. 8. The potential $\beta w_{\alpha\gamma}(R)$ between a pair of particles of species α and γ separated by distance R (measured in units of σ_{bb}) in the mixture at solvent packing fraction $\eta_s = 0$ for several values of η_c.
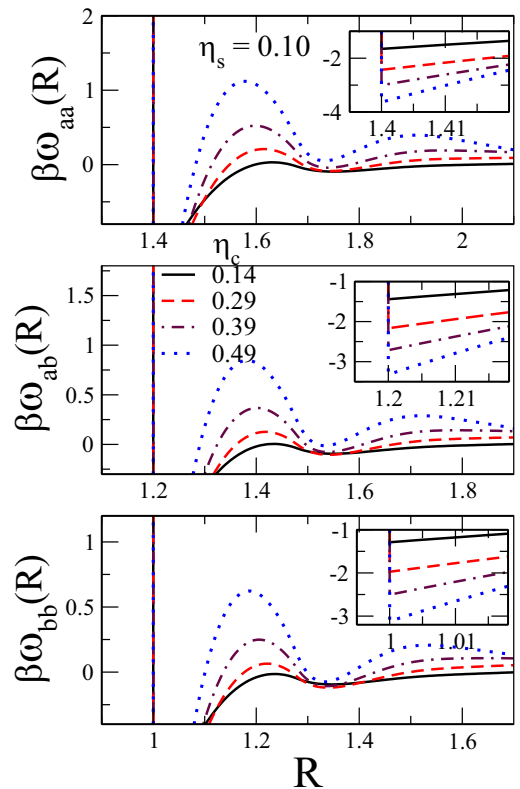

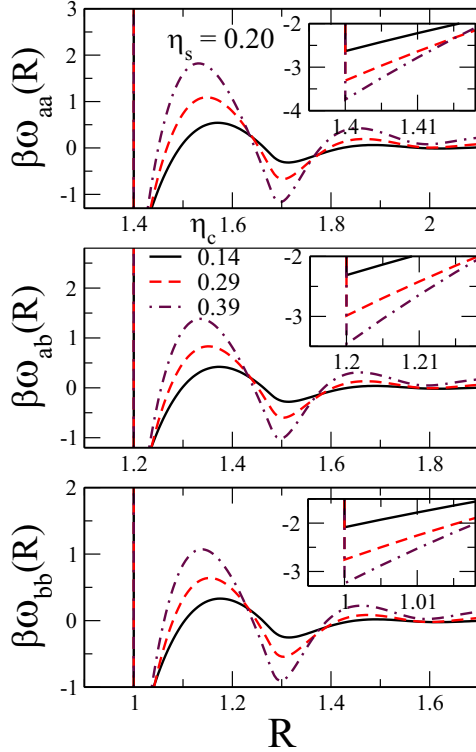FIG. 9. The same as for Fig. 8 but with $\eta_s = 0.1$.

FIG. 10. The same as for Fig. 8 but with $\eta_s = 0.2$.

Fig. 15(b) as a function of η_c/η_g where $\eta_g(\eta_s)$ (defined below) is the glass transition packing fraction at a given η_s. From these figures, it is obvious that the solvent affects the local structure of colloidal components in a significant way.

B. Activation energy barrier and the relaxation time

In Fig. 16 we plot the activation energy $\beta E^{(l)}$ as a function of η_c/η_g (the glass transition packing fraction η_g is defined below) calculated from (2.7). In the figure, symbols denote calculated values of $\beta E^{(l)}$, and the dashed lines denote fitting found using a relation,

$$\beta E^{(l)} = 1 + A\frac{(\eta_c - \bar{\eta})}{(\eta_{cr} - \eta_c)}, \qquad (4.2)$$

where $\bar{\eta}(\eta_s)$ is a value of η_c at which $\beta E^{(l)}$ is equal to 1 and η_{cr} is the value at which $\beta E^{(l)}$ diverges. In Fig. 17(a) we show the variation of η_{cr} and η_r and in Fig. 17(b) variation of A as η_s is increased. As expected, RCP η_r increases as η_s increases. We note that (4.2) gives a very good account of $\beta E^{(l)}(\eta_s)$. A fit with power law $\beta E^{(l)} = B(n^{(l)} + 1)^\delta$ is shown in Fig. 18(a) and dependence of B and δ on η_s in Fig. 18(b). Both B and δ show a nonlinear increase on increasing η_s suggesting subtle dependence of the activation barrier on number of particles in the CRC.

In Fig. 19 we compare values of τ_α/τ_0 where τ_0 is taken equal to 1 as a function of η_c for a binary mixture of species a and b when $\eta_s = 0$ with simulation results reported in Refs. [18,43]. We note that our values are in very good agreement with simulation results for $\eta_c \gtrsim 0.5$ where relaxation is dominated by activations. Since for $\eta_c \lesssim 0.5$ the dynamics is not dominated by the activation, we should not expect
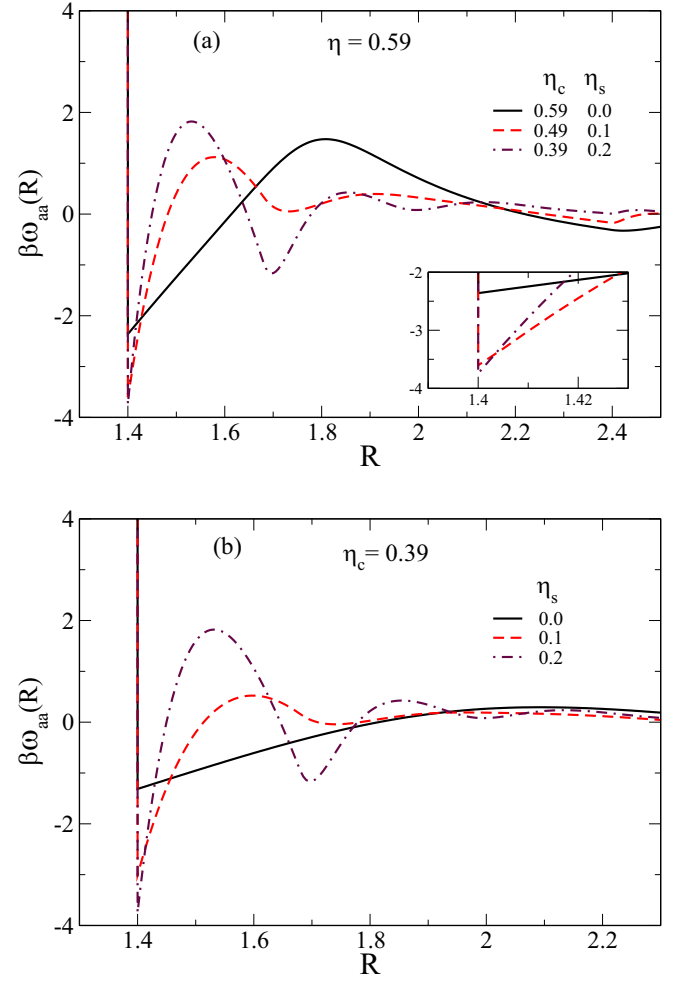
FIG. 11. Comparison of values of $\beta w_{aa}(R)$ vs R at (a) total packing fraction $\eta = 0.59$; (b) colloidal packing fraction $\eta = 0.39$ for different solvent packing fractions $\eta_s = 0.0, 0.1$ and 0.2.

agreement in the region with simulation results. In Fig. 20 we plot τ_α/τ_0 as a function of η_c for several values of η_s. We choose the value of η_c as a glass transition value η_g at which $\tau_\alpha/\tau_0 = 10^6$ and plot τ_α/τ_0 as a function of normalized packing fraction η_c/η_g in Fig. 21. This figure is an analog of the Angell plot for the molecular glass [35,38]. From the figure, we note that as η_s increases, the slope of curves of τ_α/τ_0 vs η_c/η_g decreases. This shows that as the concentration of solvent increases the hard-sphere colloidal glass behavior changes from fragile to strong. The kinetic fragility κ defined as

$$\kappa(\eta_s) = \frac{d\log_{10}(\tau_\alpha/\tau_0)}{d(\eta_c/\eta_g)}\bigg|_{\eta_c = \eta_g} = \frac{A\eta_g}{\ln 10}\frac{(\eta_{cr} - \bar{\eta})}{(\eta_{cr} - \eta_g)^2} \qquad (4.3)$$

is plotted in Fig. 22. We note that κ varies strongly with η_s and changes from $\kappa \simeq 92$ for $\eta_s = 0$ down to $\kappa \simeq 22$ for $\eta_s = 0.2$. Thus, we find the system of hard spheres dispersed in a solvent of small-sized hard spheres displays a large variation in the kinetic fragility on changing the concentration of the solvent.
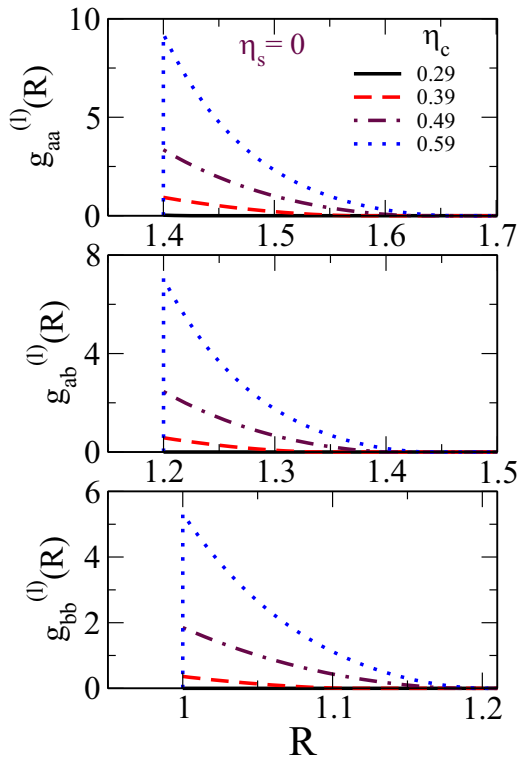
FIG. 12. Plot of $g_{\alpha\gamma}^{(l)}(R)$ as a function R at $\eta_s = 0$ for the several values of η_c.
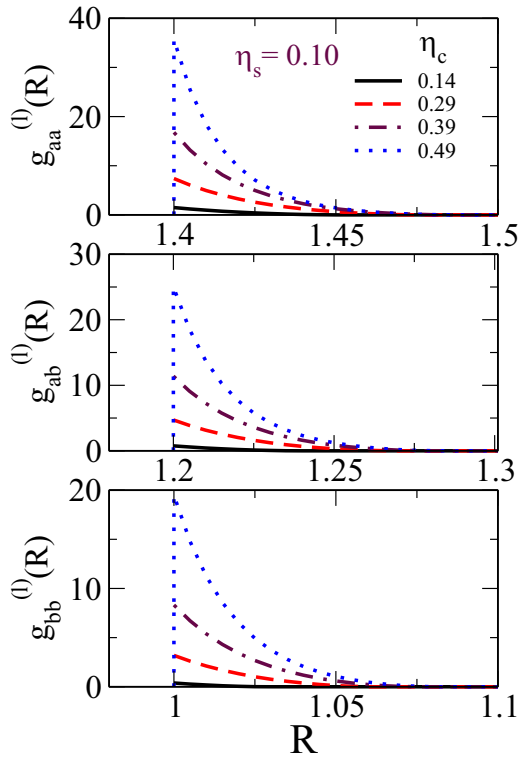

FIG. 13. The same as for Fig. 12 but with $\eta_s = 0.1$.
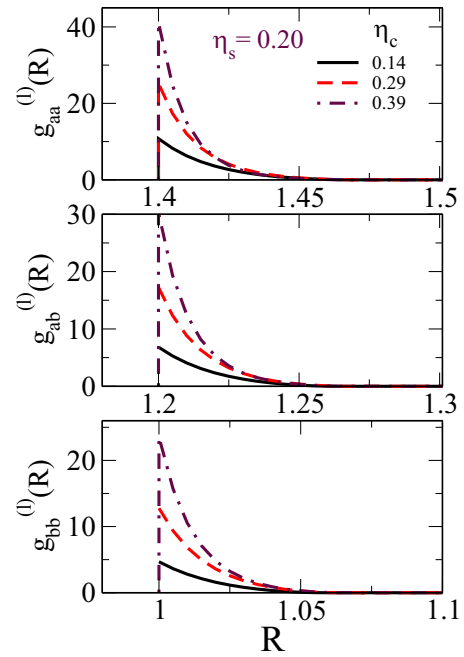

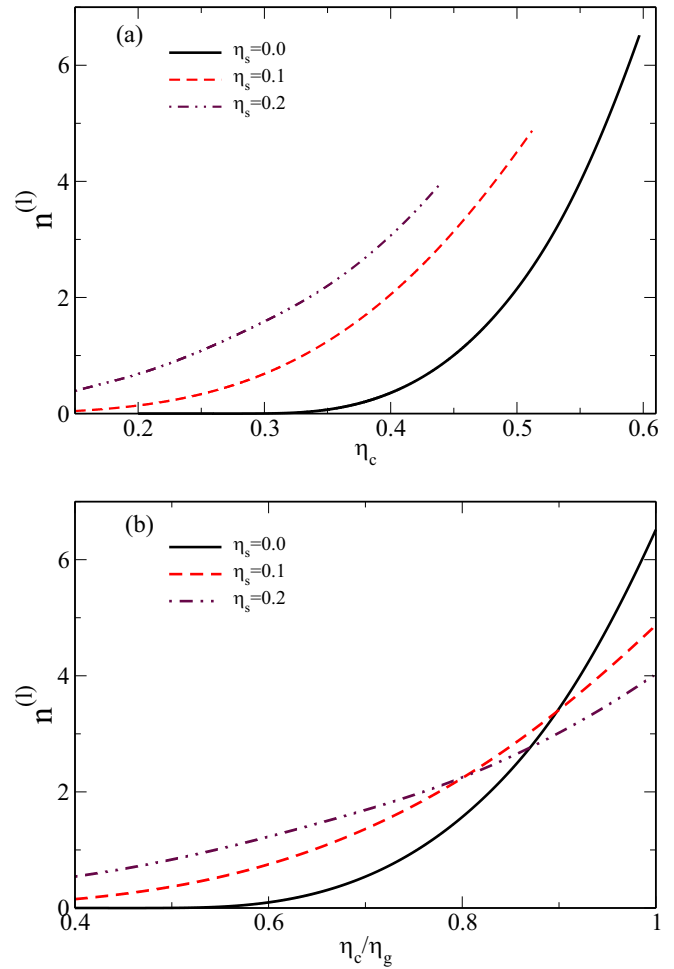FIG. 14. The same as for Fig. 12 but with $\eta_s = 0.2$.

FIG. 15. Number of long-lived particles (l particles) $n^{(l)}$ that form CRC (a) as a function of η_c; (b) as a function of η_c/η_g, where η_g is a glass transition packing fraction at which $\tau_\alpha/\tau_0 = 10^6$.
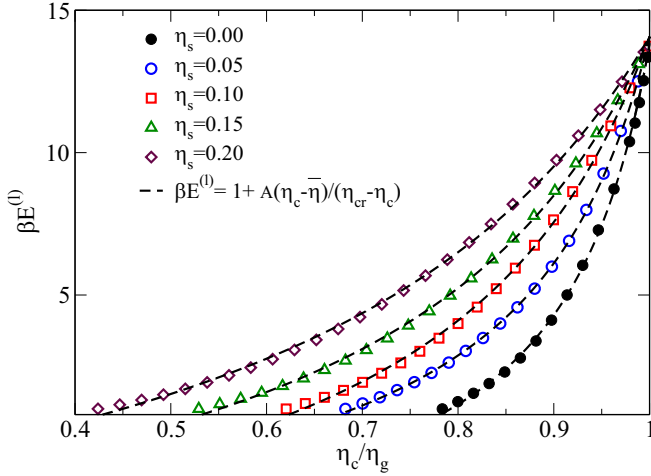
FIG. 16. The activation energy $\beta E^{(l)}$ as a function of η_c/η_g calculated from (2.7). In the figure symbols denote calculated values of $\beta E^{(l)}$, and the dashed lines denote fitting found using a relation (4.2), where $\bar{\eta}(\eta_s)$ is a value of η_c at which $\beta E^{(l)}$ is equal to 1, and η_{cr} is the value at which $\beta E^{(l)}$ diverges.

V. SUMMARY AND CONCLUSIONS

In this paper, we develop a theory to calculate the structure and activated dynamics of colloidal components in a size-asymmetric ternary mixture. In particular, we present the results for a system of a binary mixture of hard-sphere colloidal particles dispersed in a solvent of much smaller-sized hard spheres. On increasing the concentration of colloidal particles at a fixed concentration of solvent, the system exhibits a dramatic rise in structural relaxation time τ_α, a feature that has many hallmarks of the glass transition in molecular materials. For several decades, colloids have served as a valuable model system for understanding the glass transition in molecular systems [2–4]. The large size of colloidal particles makes it possible to study both structure and dynamics with light scattering and imaging [3,33,34]. However, due to technical limitations related to optical resolutions, observations are often limited only to colloidal components; the solvent component remains unobserved. Thus, apart from the need of coarse graining due to the coexistence of widely different time and length scales, integrating out of the solvent degrees of freedom and reduction of the system to effective binary mixture of colloidal particles is in sync with the restricted nature of experimental observations.
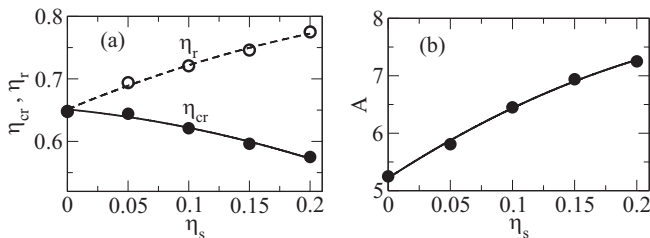

FIG. 17. (a) Variation of η_{cr} (filled circles) and η_r (open circles) as a function of η_s. (b) Variation of A as a function of η_s.
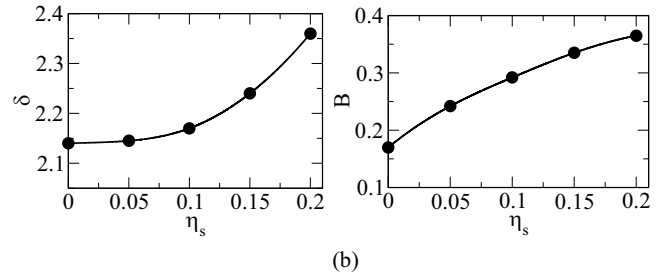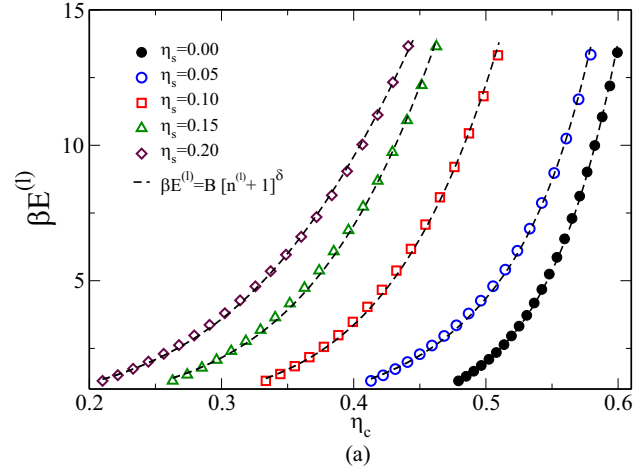

FIG. 18. (a) Plot of the activation energy $\beta E^{(l)}$ as a function of η_c. The symbols represent values found from the calculation, and the dashed line represents a fit with power law $\beta E^{(l)} = B(n^{(l)} + 1)^\delta$, where $n^{(l)}$ is the number of bonds in a CRC (see Fig. 15) and in (b) dependence of B and δ on η_s. Both B and δ show a nonlinear increase on increasing η_s.
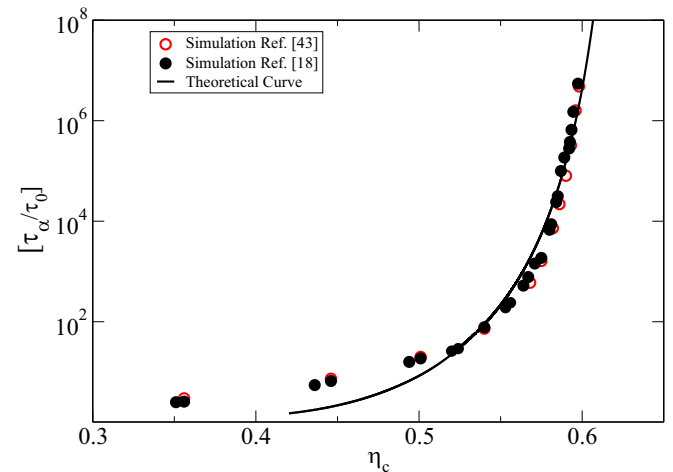
FIG. 19. Comparison of calculated values (solid line) of τ_α/τ_0 where τ_0 is taken equal to 1 as a function of η_c for a binary mixture of species a and b when $\eta_s = 0$ with simulation values (open circles [43] and filled circles [18]). Our values are in very good agreement with simulation results for $\eta_c \gtrsim 0.5$ where relaxation is dominated by activations: For $\eta_c \lesssim 0.5$ agreement is not expected as the dynamics in this region are dominated by other than the activation which has not been considered in the present paper.
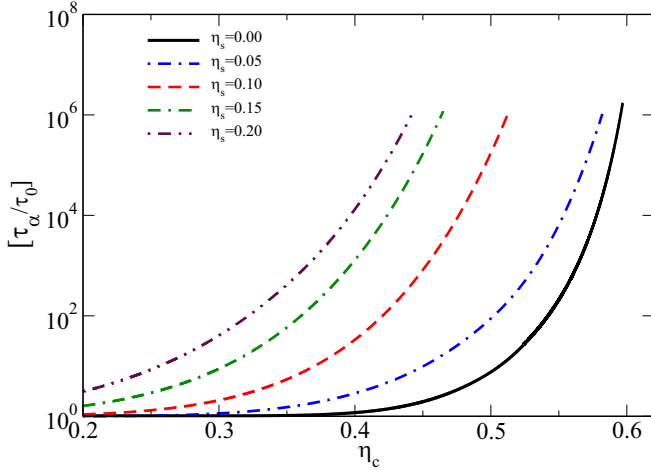
FIG. 20. Plot of the relaxation time τ_α/τ_0 as a function of η_c for several values of η_s.

The coarse graining used to trace out solvent degrees of freedom from the grand partition function of the ternary mixture is described in Sec. III. This method is based on density functional formalism of density profile and the grand potential of the solvent and is an extension to ternary mixture of a method developed in Ref. [53] for a binary mixture. In the coarse-grained system, colloidal particles interact via effective potential that consists of bare plus solvent-induced interaction. A self-consistent iterative method summarized in the Appendix is used to calculate values of correlation functions $\bar{c}_{\alpha s}$, $g_{\alpha s}$, and $g_{\alpha \gamma}$, and of the effective potential $\beta U_{\alpha \gamma}(R)$. These quantities can be used to describe the structural and thermodynamic properties of the system. In particular, $g_{\alpha s}$ gives the distribution of solvent particles around a colloidal particle of species α.
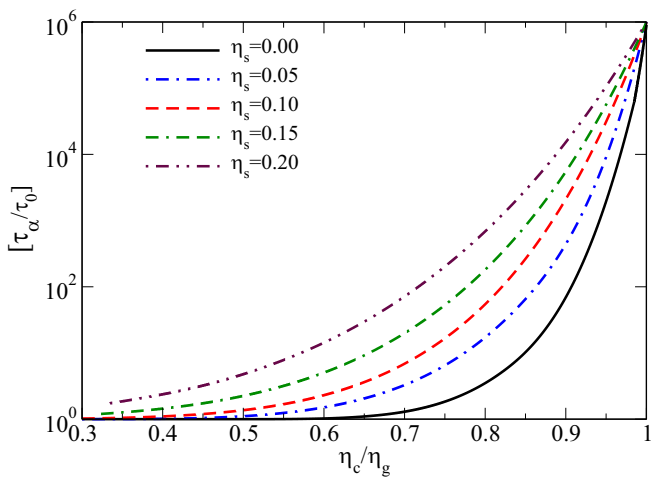

FIG. 21. Angell plot of τ_α/τ_0 as a function of normalized packing fraction η_c/η_g at different solvent packing fractions η_s. At lower η_s, the relaxation time exhibits a sharp growth upon increasing η_c, i.e., a feature of a fragile glass former, whereas at higher η_s, the relaxation time display relatively slow growth with η_c, suggesting a strong glass former.
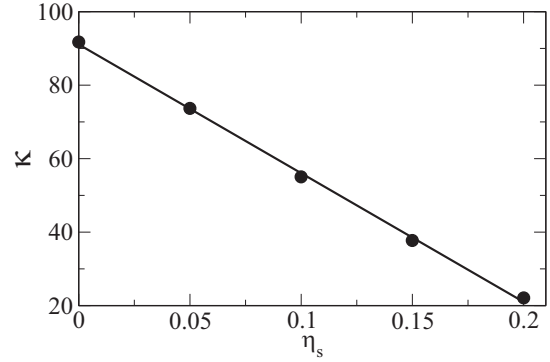

FIG. 22. Variation of kinetic fragility κ as a function of η_s.

The theory outlined in Sec. II uses the static pair correlation function $g_{\alpha \gamma}(R)$ to calculate the number of particles which form (nonchemical) bonds with a central particle. The number of these particles increases rapidly on lowering the temperature and on increasing the density due to an increase in the number of shells surrounding the central particle and an increase in values of maximum and minimum of each shell (see Fig. 1). Depending upon their energies the bonded particles are divided into two subsets; (i) particles which form long-lived ($l-$) bonds and remain trapped in the potential shells, at least, until the activated processes can restore diffusive motion, and (ii) particles which form metastable ($m-$) bonds with the central particles and exhibit wide ranges of spatial and temporal dynamics. A CRC is formed by a central particle with its neighbors of (l) particles. The particles in a CRC are distributed in coordination shells surrounding the central particle and may share the space with metastable particles. The CRC differs from the Adam and Gibbs [58] "cooperatively rearranging region" which is taken to be a compact structure [58,59]. For an event of relaxation to take place, the CRC has to reorganize irreversibly, the energy involved in this rearrangement is the energy with which the central particle is bonded with l particles. It may, however, be noted that a CRC is embedded at the center of a much larger cluster of m particles. Since m particles are loosely bonded with the central particle, they move individually or in a group of a few particles on a timescale much smaller than τ_α without affecting the structure of CRC. However, when the CRC reorganizes at timescales commensurate with τ_α, by moving its particles it may trigger the reorganization of all particles of the cluster turning into a large cluster of mobile particles. Therefore, in simulation as well as in experiments, one may see relaxation governed by rapid sporadic events characterized by the emergence of a relatively large and a compact cluster of mobile particles [60,61].

Thus, in addition to the cooperativity of relaxation defined in terms of the number of particles in a CRC, a larger and relatively more compact cluster consisting of l and m particles provides another length scale of the glassy dynamics. This length scale seems to be in agreement with the dynamics heterogeneity measured by the four-point susceptibility function $\chi_4(t)$ [62–65]. The function $\chi_4(t)$ at its maximum measures the volume on which the dynamical processes relevant to structural relaxation at time $t \simeq \tau_\alpha$ are correlated. However,

values of $\chi_4(t)$ determined from simulations are found (see, e.g., Ref. [65]) to depend on the microscopic equation of motion of the system (Newtonian vs Brownian) and on the statistical ensemble. These subtle issues make the analysis of the four-point susceptibilities somewhat ambiguous, especially when estimates of cooperative lengths of relaxation are sought.

A comparison of values of τ_α/τ_0 as a function of packing fraction η_c for a binary mixture of species a and b (see Fig. 19) shows that our theory gives a very good account of the activated dynamics of glass-forming fluids. When solvent is added to the system the dynamics get affected. The solvent particles which distribute around colloidal particles affect the local structure and, therefore, the cage [potential well $\beta w_{\alpha\gamma}(R)$] that arrests particles to form CRC. This is evident from Fig. 15. where number of particles in a CRC is plotted as a function of η_c as well as a function of η_c/η_g at $\eta_s = 0$, 0.1, and 0.2. From the results of these and other figures, we conclude that solvent has a significant effect on the size of the CRC and, therefore,on the activated dynamics and on the relaxation time τ_α.

Taken together, the results reported above show that solvent can be used as a control parameter to fine-tune the microscopic structural ordering of colloidal particles and, therefore, the emergence and size of cooperatively reorganizing cluster (CRC) that governs the glassy dynamics. Our findings suggest that a small variation in the concentration of the solvent can create a bigger change in kinetic fragility in hard-sphere colloidal systems which highlights a wide variation in behavior, ranging from fragile to strong glasses. The underlying cause for this change is the change in the size (number of particles) of CRC formed by localized particles. Based on the results reported in previous papers [44–46] and this one we conclude that the CRC which is determined from the static pair correlation function and the fluctuations embedded in the system is probably the sole player in the physics of glass transition.

ACKNOWLEDGMENT

APPENDIX

A self-consistent iterative procedure used in calculation is based on the method described in Ref. [53]. For known values of $\tilde{S}_{ss}(\vec{r}, \vec{r}')$ and $h_{\alpha\gamma}(R)$ Eq. ((3.24)) is solved with the help of a suitable closure relation to find $h_{\alpha s}(r)$ and $\bar{c}_{\alpha s}(r)$. Equation ((3.24)) is rewritten as

$$h_{\alpha s}(r) = \sum_\gamma \left[\int d\vec{r}' \tilde{S}_{ss}(\vec{r}, \vec{r}') \bar{c}_{\gamma s}(\vec{r}') + \rho_s \right.$$
$$\left. \times \int d\vec{r}' \int d\vec{R}_\gamma \tilde{S}_{ss}(\vec{r}, \vec{r}') \bar{c}_{\gamma s}(\vec{r}', \vec{R}_\gamma) h_{\alpha\gamma}(\vec{R}_\alpha, \vec{R}_\gamma) \right],$$
(A1)

where

$$\tilde{S}_{ss}(\vec{r}, \vec{r}') = \int_0^1 d\lambda \, S_{ss}(\vec{r}, \vec{r}'; \lambda),$$

and

$$S_{ss}(\vec{r}, \vec{r}'; \lambda) = \delta(|\vec{r} - \vec{r}'|) + \rho_s(\lambda) h_{ss}(\vec{r}, \vec{r}'; \lambda). \quad (A2)$$

Since volume $\eta_c V$ occupied by colloidal particles is not available to solvent particles, the density of solvent in the mixture effectively becomes $\rho_s^* = \rho_s/(1 - \eta_c)$. In view of this we define $\rho_s(\lambda) = \rho_s/(1 - \lambda\eta_c)$ and calculate $\tilde{S}_{ss}$ from (A2). Thus,

$$\tilde{S}_{ss}(\vec{r}, \vec{r}') = \int_0^1 d\lambda \{\delta(\bar{r} - \bar{r}') + \rho_s(\lambda) h_{ss}[\vec{r}, \vec{r}'; \rho_s(\lambda)]\},$$

$$= S_{ss}(\vec{r}, \vec{r}') + \int_0^1 d\lambda \{\rho_s(\lambda) h_{ss}[\vec{r}, \vec{r}'; \rho_s(\lambda)]$$
$$- \rho_s h_{ss}(\vec{r}, \vec{r}'; \rho_s)\}, \quad (A3)$$

where the first term on the right-hand side of the above equation corresponds to the linear response approximation and the second term correction to the density-density correlation function of solvent due to the presence of colloidal particles.

Equation (A1) now has three unknowns; $h_{\alpha s}(r)$, $\bar{c}_{\alpha s}(r)$, and $h_{\alpha\gamma}(R)$. The function $h_{\alpha\gamma}(R)$ is calculated from effective potential $U_{\alpha\gamma}(R)$ using the OZ equation of binary mixtures. To solve (A1) we used closure relation [53],

$$g_{\alpha s}(r) = 1 + h_{\alpha s}(r) = g_{\alpha s}^{(p)}(r)\left[1 + Y_{\alpha s}(r) - Y_{\alpha s}^{(p)}(r)\right], \quad (A4)$$

where $Y_{\alpha s}(r) = h_{\alpha s}(r) - \bar{c}_{\alpha s}(r)$. The quantities with superscript (p) represent values of previous colloidal density ρ_α. In the limit $\rho_\alpha \to 0$ (A1) reduces to

$$h_{\alpha s}(r) = \sum_\gamma \int d\vec{r}' \tilde{S}_{\gamma s}(\vec{r}, \vec{r}') \bar{c}_{\gamma s}(\vec{r}'), \quad (A5)$$

which is the OZ equation. It is solved using a closure relation for $h_{\alpha s}^{(0)}(r)$ and $c_{\alpha s}^{(0)}(r)$ where the superscript zero is used to indicate that these values belong to the limit $\rho_\alpha \to 0$. As ρ_γ is increased the role of second term of (A1) becomes important. We have formed a grid of ρ_γ with small spacing and used results of lower density as input to calculate for higher density using relation (A1). For the determination of $h_{\alpha\gamma}(R)$ from known $U_{\alpha\gamma}(R)$ we used the monocomponent OZ equation,

$$h_{\alpha\gamma}(R) = c_{\alpha\gamma}(R) + \sum_k \rho_k \int d\bar{R}' \, h_{\alpha k}(|\bar{R} - \bar{R}'|) c_{k\gamma}(R'), \quad (A6)$$

and a closure relation,

$$g_{\alpha\gamma}(R) = g_{\alpha\gamma}^{(bm)}(R) \exp\left[-\left\{v_{\alpha\gamma}(R) - v_{\alpha\gamma}^{(bm)}(R)\right\}\right.$$
$$\left. + Y_{\alpha\gamma}(R) - Y_{\alpha\gamma}^{(bm)}(R)\right]. \quad (A7)$$

which is the RHNC relation where reference terms correspond to binary colloidal mixture interacting via pair potential $u_{\alpha\gamma}(R)$. The value of $g_{\alpha\gamma}^{(bm)}(R)$ is found from IET using the Rogers-Young [57] closure relation as described in the text.

The functions $\bar{\chi}_{ss}(\vec{r}, \vec{r}')$ are calculated from the relation,

$$\bar{\chi}_{ss}(\vec{r}, \vec{r}') = 2\rho_s \int_0^1 d\lambda(1 - \lambda)[\delta(|\vec{r} - \vec{r}'|)$$
$$+ \rho_s(\lambda) h_{ss}(\vec{r}, \vec{r}'; \lambda)]. \quad (A8)$$

[1] G. Parisi and F. Zamponi, Mean-field theory of hard sphere glasses and jamming, Rev. Mod. Phys. **82**, 789 (2010).

[2] P. Pusey and W. van Megen, Phase behaviour of concentrated suspensions of nearly hard colloidal spheres, Nature (London) **320**, 340 (1986).

[3] G. L. Hunter and E. R. Weeks, The physics of the colloidal glass transition, Rep. Prog. Phys. **75**, 066501 (2012).

[4] P. J. Lu and D. A. Weitz, Colloidal particles: Crystals, glasses, and gels, Annu. Rev. Condens. Matter Phys. **4**, 217 (2013).

[5] S. Torquato, T. M. Truskett, and P. G. Debenedetti, Is Random Close Packing of Spheres Well Defined? Phys. Rev. Lett. **84**, 2064 (2000).

[6] C. S. O'Hern, S. A. Langer, A. J. Liu, and S. R. Nagel, Random Packings of Frictionless Particles, Phys. Rev. Lett. **88**, 075507 (2002).

[7] R. D. Kamien and A. J. Liu, Why is Random Close Packing Reproducible? Phys. Rev. Lett. **99**, 155501 (2007).

[8] I. Biazzo, F. Caltagirone, G. Parisi, and F. Zamponi, Theory of Amorphous Packings of Binary Mixtures of Hard Spheres, Phys. Rev. Lett. **102**, 195701 (2009).

[9] R. Mari, F. Krzakala, and J. Kurchan, Jamming versus Glass Transitions, Phys. Rev. Lett. **103**, 025701 (2009).

[10] P. Chaudhuri, L. Berthier, and S. Sastry, Jamming Transitions in Amorphous Packings of Frictionless Spheres Occur over a Continuous Range of Volume Fractions, Phys. Rev. Lett. **104**, 165701 (2010).

[11] S. Torquato and F. H. Stillinger, Jammed hard-particle packings: From kepler to bernal and beyond, Rev. Mod. Phys. **82**, 2633 (2010).

[12] S. Wilken, R. E. Guerra, D. Levine, and P. M. Chaikin, Random Close Packing as a Dynamical Phase Transition, Phys. Rev. Lett. **127**, 038002 (2021).

[13] A. Zaccone, Explicit analytical solution for random close packing in $d = 2$ and $d = 3$, Phys. Rev. Lett. **128**, 028002 (2022).

[14] W. van Megen, T. C. Mortensen, S. R. Williams, and J. Müller, Measurement of the self-intermediate scattering function of suspensions of hard spherical particles near the glass transition, Phys. Rev. E **58**, 6073 (1998).

[15] T. G. Mason and D. A. Weitz, Linear Viscoelasticity of Colloidal Hard Sphere Suspensions near the Glass Transition, Phys. Rev. Lett. **75**, 2770 (1995).

[16] W. K. Kegel and A. van Blaaderen, Direct observation of dynamical heterogeneities in colloidal hard-sphere suspensions, Science **287**, 290 (2000).

[17] E. R. Weeks, J. C. Crocker, A. C. Levitt, A. Schofield, and D. A. Weitz, Three-dimensional direct imaging of structural relaxation near the colloidal glass transition, Science **287**, 627 (2000).

[18] G. Brambilla, D. El Masri, M. Pierno, L. Berthier, L. Cipelletti, G. Petekidis, and A. B. Schofield, Probing the Equilibrium Dynamics of Colloidal Hard Spheres above the Mode-Coupling Glass Transition, Phys. Rev. Lett. **102**, 085703 (2009).

[19] M. Fasolo and P. Sollich, Equilibrium Phase Behavior of Polydisperse Hard Spheres, Phys. Rev. Lett. **91**, 068301 (2003).

[20] P. Sollich and N. B. Wilding, Crystalline Phases of Polydisperse Spheres, Phys. Rev. Lett. **104**, 118302 (2010).

[21] E. Zaccarelli, C. Valeriani, E. Sanz, W. C. K. Poon, M. E. Cates, and P. N. Pusey, Crystallization of Hard-Sphere Glasses, Phys. Rev. Lett. **103**, 135704 (2009).

[22] E. Zaccarelli, S. M. Liddle, and W. C. K. Poon, On polydispersity and the hard sphere glass transition, Soft Matter **11**, 324 (2015).

[23] D. Heckendorf, K. J. Mutch, S. U. Egelhaaf, and M. Laurati, Size-Dependent Localization in Polydisperse Colloidal Glasses, Phys. Rev. Lett. **119**, 048003 (2017).

[24] A. Imhof and J. K. G. Dhont, Experimental Phase Diagram of a Binary Colloidal Hard-Sphere Mixture with a Large Size Ratio, Phys. Rev. Lett. **75**, 1662 (1995).

[25] A. J. Moreno and J. Colmenero, Anomalous dynamic arrest in a mixture of large and small particles, Phys. Rev. E **74**, 021409 (2006).

[26] A. J. Moreno and J. Colmenero, Relaxation scenarios in a mixture of large and small spheres: Dependence on the size disparity, J. Chem. Phys. **125**, 164507 (2006).

[27] R. Juárez-Maldonado and M. Medina-Noyola, Theory of dynamic arrest in colloidal mixtures, Phys. Rev. E **77**, 051503 (2008).

[28] T. Voigtmann, Multiple glasses in asymmetric binary hard spheres, Europhys. Lett. **96**, 36006 (2011).

[29] E. Martinez-Sotelo, M. A. Escobedo-Sánchez, and M. Laurati, Effect of size disparity on the structure and dynamics of the small component in concentrated binary colloidal mixtures, J. Chem. Phys. **151**, 164504 (2019).

[30] S. R. Williams and W. van Megen, Motions in binary mixtures of hard colloidal spheres: Melting of the glass, Phys. Rev. E **64**, 041502 (2001).

[31] G. Foffi, W. Götze, F. Sciortino, P. Tartaglia, and T. Voigtmann, Mixing Effects for the Structural Relaxation in Binary Hard-Sphere Liquids, Phys. Rev. Lett. **91**, 085701 (2003).

[32] W. Götze and T. Voigtmann, Effect of composition changes on the structural relaxation of a binary mixture, Phys. Rev. E **67**, 021502 (2003).

[33] T. Sentjabrskaja, E. Babaliari, J. Hendricks, M. Laurati, G. Petekidis, and S. U. Egelhaaf, Yielding of binary colloidal glasses, Soft Matter **9**, 4524 (2013).

[34] J. Hendricks, R. Capellmann, A. B. Schofield, S. U. Egelhaaf, and M. Laurati, Different mechanisms for dynamical arrest in largely asymmetric binary mixtures, Phys. Rev. E **91**, 032308 (2015).

[35] C. A. Angell, Formation of glasses from liquids and biopolymers, Science **267**, 1924 (1995).

[36] C. A. Angell, K. L. Ngai, G. B. McKenna, P. F. McMillan, and S. W. Martin, Relaxation in glassforming liquids and amorphous solids, J. Appl. Phys. **88**, 3113 (2000).

[37] A. D. Phan and K. S. Schweizer, Theory of activated glassy dynamics in randomly pinned fluids, J. Chem. Phys. **148**, 054502 (2018).

[38] H. W. Cho, M. L. Mugnai, T. R. Kirkpatrick, and D. Thirumalai, Fragile-to-strong crossover, growing length scales, and dynamic heterogeneity in wigner glasses, Phys. Rev. E **101**, 032605 (2020).

[39] J. Mattsson *et al.*, Soft colloids make strong glasses, Nature (London) **462**, 83 (2009).

[40] C. Alba-Simionesco and G. Tarjus, A perspective on the fragility of glass-forming liquids, Journal of Non-Crystalline Solids: X **14**, 100100 (2022).

[41] I. Tah and S. Karmakar, Kinetic fragility directly correlates with the many-body static amorphous order in glass-forming liquids, Phys. Rev. Mater. **6**, 035601 (2022).

[42] S. E. Abraham, S. M. Bhattacharrya, and B. Bagchi, Energy Landscape, Antiplasticization, and Polydispersity Induced Crossover of Heterogeneity in Supercooled Polydisperse Liquids, Phys. Rev. Lett. **100**, 167801 (2008).

[43] L. Berthier and T. A. Witten, Glass transition of dense fluids of hard and compressible spheres, Phys. Rev. E **80**, 021502 (2009).

[44] A. Singh and Y. Singh, Super-Arrhenius behavior of molecular glass formers, Phys. Rev. E **99**, 030101(R) (2019).

[45] A. Singh, S. M. Bhattacharyya, and Y. Singh, Emergence of cooperatively reorganizing cluster and super-Arrhenius dynamics of fragile supercooled liquids, Phys. Rev. E **103**, 032611 (2021).

[46] A. Singh and Y. Singh, How attractive and repulsive interactions affect structure ordering and dynamics of glass-forming liquids, Phys. Rev. E **103**, 052105 (2021).

[47] A. Ayadim and S. Amokrane, Phase transitions in highly asymmetric binary hard-sphere fluids: Fluid-fluid binodal from a two-component mixture theory, Phys. Rev. E **74**, 021106 (2006).

[48] S. Amokrane, A. Ayadim, and J. G. Malherbe, Structure of highly asymmetric hard-sphere mixtures: An efficient closure of the Ornstein-Zernike equations, J. Chem. Phys. **123**, 174508 (2005).

[49] S. B. Yuste, A. Santos, and M. López de Haro, Depletion potential in the infinite dilution limit, J. Chem. Phys. **128**, 134507 (2008).

[50] D. J. Ashton, N. B. Wilding, R. Roth, and R. Evans, Depletion potentials in highly size-asymmetric binary hard-sphere mixtures: Comparison of simulation results with theory, Phys. Rev. E **84**, 061136 (2011).

[51] E. López-Sánchez, C. D. Estrada-Álvarez, G. Pérez-Ángel, J. M. Méndez-Alcaraz, P. González-Mozuelos, and R. Castañeda-Priego, Demixing transition, structure, and depletion forces in binary mixtures of hard-spheres: The role of bridge functions, J. Chem. Phys. **139**, 104908 (2013).

[52] M. Yadav and Y. Singh, The solvent mediated interaction potential between solute particles: Theory and applications, Soft Matter **16**, 9780 (2020).

[53] M. Yadav and Y. Singh, Coarse-grained hamiltonian and effective one component theory of colloidal suspensions, J. Mol. Liq. **366**, 120233 (2022).

[54] J. Callaham and J. Machta, Population annealing simulations of a binary hard-sphere mixture, Phys. Rev. E **95**, 063315 (2017).

[55] Y. Singh, Density-functional theory of freezing and properties of the ordered phase, Phys. Rep. **207**, 351 (1991).

[56] J.-P. Hansen and I. R. McDonald, *Theory of Simple Liquids*, (Academic, Burlington, VT, 2006).

[57] F. J. Rogers and D. A. Young, New, thermodynamically consistent, integral equation for simple fluids, Phys. Rev. A **30**, 999 (1984).

[58] G. Adam and J. H. Gibbs, On the temperature dependence of cooperative relaxation properties in glass-forming liquids, J. Chem. Phys. **43**, 139 (1965).

[59] J.-P. Bouchaud and G. Biroli, On the Adam-Gibbs-Kirkpatrick-Thirumalai-Wolynes scenario for the viscosity increase in glasses, J. Chem. Phys. **121**, 7347 (2004).

[60] G. A. Appignanesi, J. A. Rodríguez Fris, R. A. Montani, and W. Kob, Democratic Particle Motion for Metabasin Transitions in Simple Glass Formers, Phys. Rev. Lett. **96**, 057801 (2006).

[61] J. A. R. Fris, G. A. Appignanesi, and E. R. Weeks, Experimental Verification of Rapid, Sporadic Particle Motions by Direct Imaging of Glassy Colloidal Systems, Phys. Rev. Lett. **107**, 065704 (2011).

[62] C. Dasgupta, A. V. Indrani, S. Ramaswamy, and M. K. Phani, Is there a growing correlation length near the glass transition? Europhys. Lett. **15**, 307 (1991).

[63] C. Toninelli, M. Wyart, L. Berthier, G. Biroli, and J.-P. Bouchaud, Dynamical susceptibility of glass formers: Contrasting the predictions of theoretical scenarios, Phys. Rev. E **71**, 041505 (2005).

[64] D. El Masri, L. Berthier, and L. Cipelletti, Subdiffusion and intermittent dynamic fluctuations in the aging regime of concentrated hard spheres, Phys. Rev. E **82**, 031503 (2010).

[65] L. Berthier and G. Biroli, Theoretical perspective on the glass transition and amorphous materials, Rev. Mod. Phys. **83**, 587 (2011).